Nonlinear Dyn (2017) 88:883–892
DOI 10.1007/s11071-016-3282-3

ORIGINAL PAPER

Analysis on nonlinear turning motion of multi-spherical soft robots

Yanqiong Fei · Wu Pang

Received: 20 July 2016 / Accepted: 9 December 2016 / Published online: 23 December 2016

Abstract A modular multi-spherical soft robot, which consists of five deformable spherical cells, two friction feet, the electromagnetic valves and the control systems, is constructed. According to the deflating action and the inflating action of the spherical cells, the size and the shape of each spherical cell can be changed. With two friction feet sticking with the ground in turn, the soft robot can move forwards, make a turning motion and avoid the obstacle. This paper creates a nonlinear relation between the pressure P and the inflation radius (r) at different original radii (r_0) and obtains the inflation or deflation velocity v_r. Six inflating and deflating steps to finish the turning motion are presented. Based on the geometric relationship between the inflation radius (r) and the original radius (r_0) of each cell, the nonlinear turning process is described to control the center positions (x, y, z) of the spherical cell. Last, a simulation and an experiment of five spherical cells are shown to emulate the turning process. Experiment results show that the robot has a maximum turning capability of 20° in one period.

Y. Fei (✉) · W. Pang
Research Institute of Robotics, Shanghai Jiaotong University, Dongchuan Road 800, Shanghai 200240, People's Republic of China
e-mail: fyq@sjtu.edu.cn

Y. Fei
School of Automation, Hangzhou Dianzi University, Hangzhou Shi, China

Keywords Turning motion · Soft robot · Spherical cell · Nonlinear analysis

1 Introduction

Soft robots are a type of new robots, and research on them is only at the initial stage. The main characteristic of soft robots is their low resistance to stress forces. Like some animals, they can morph among different shapes to move forwards. Soft robots have many advantages and priorities to traditional rigid robots. They can change their sizes and shapes in large range and have wide potential applications in detection, exploration, succor and medicine. They can safely interact with humans and natural environments [1]. They can go through an obstacle, which can allow low height only. The soft robot can better mimic the moving mode of natural living creatures which can adapt to environments [2,3].

Soft robots use changes in pressure of liquid or air to move in a unique way. Onal presented an approach to create a bio-inspired soft robotic snake that could undulate in a similar way to its biological counterpart using pressure for actuation power, without human intervention [4]. Cecilia [5] invented octopus-inspired soft arms, which could bend like real arms of people. Manti developed a soft robotic gripper with three fingers. It could achieve passive adaption to target varying in shape, size and material during grasping, which simplified the controlling system [6]. Fei analyzed the

nonlinear dynamic moving process with the deflating and inflating modes [3,7]. Additionally, some different moving modes such as a caterpillar-inspired moving mode [8–11] and a deformational jumping and crawling moving mode were presented. The crawling soft robot was pushed by walking with four legs, which was reflection of four-foot animals [12]. Teruyoshi built up a model of a crawling soft robot by referring to the crawling mode of a snail. The snail robot borrowed the forces created by the difference of the pressure in the body and outside [13]. They are all analogies of the nature. In all cases, the mechanical motion is driven by external stimuli. Koh [14] employed smart structures and actuators and proposed a deformable wheeled robot that could change the shape of the wheel depending on the obstacles. The robot imitated the locomotion mechanism of the Amoeba, actuated by the IPMC (ionic polymer–metal composites) actuators. The IPMC actuators pasted on the skin of the robot and stimulated by regular control signals could make the robot move forwards, backwards, enter the narrow holes [15]. Shepherd used the explosive combustion of hydrocarbons triggered by an electrical spark to cause a soft robot to jump over obstacles. The use of explosions for actuation was compatible with soft machines. Explosive power allowed a soft robot to jump 30 times its height with an initial speed of 3.6 m/s [16]. Huang [17] designed and fabricated a microsoft swimming robot with both powering and controlling functions provided by remote light, which did not carry any electronic devices and batteries. However, the research on the nonlinear turning motion and obstacle avoidance of the soft robot is less.

In this paper, we present one kind of deformable spherical modular soft robot. This kind of soft robot can make a turning motion to avoid the obstacle and go through the hole narrower than its body size. The nonlinear relation between the pressure P and the inflation radius (r) at different original radii (r_0), and the inflation and deflation velocity v_r are obtained. According to the deflating and inflating actions of the spherical cells, the size and the shape of each spherical cell can be changed. With the friction feet sticking with the ground in turn, the motion can be finished. With six kinds of different steps and constraint conditions, the soft robot can make a turning motion. A simulation and an experiment of five spherical cells are shown to emulate the turning process in a period.

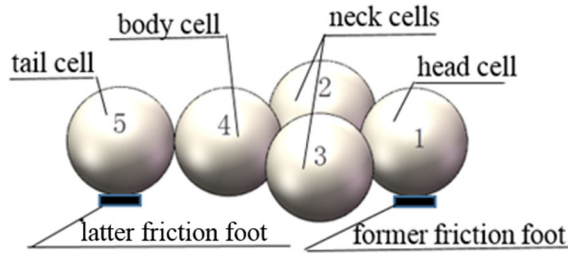

Fig. 1 Structure of the modular soft robot

2 Modular soft robot design

2.1 System structure

Modular soft robot, which consists of four spherical cells and two friction feet, can move forwards according to the deflating action and the inflating action of each spherical cell. However, the soft robot only with four spherical cells cannot provide the deflection angle; thus, it cannot turn even if it encounters obstacles. According to analyses and experiments, five spherical cells are the basic turning motion unit of modular soft robots (Fig. 1). In the paper, a five-spherical-cell soft robot system is discussed. The approach proposed can be extended to a robot made of more than 5 cells. Since the spherical cells can deflate and inflate, this kind of soft robot has the advantage of changing its size, which is not all the soft robots can do. When this robot meets a narrow hole, it can reduce the maximum inflation radius r to go through the hole, which is narrower or smaller than the maximum size of the soft robot.

The five-spherical-cell soft robot consists of a head cell (Cell 1), a tail cell (Cell 5), two neck cells (Cell 2 and Cell 3), a body cell (Cell 4), a former friction foot k_1 and a latter friction foot k_2 (Fig. 1). The former friction foot sticks with the bottom of Cell 1, and the latter friction foot sticks with the bottom of Cell 5. Each modular cell is a rubber-like spherical thin shell. According to the appropriate deflating or inflating action of each spherical cell and two friction feet sticking with the ground in turn, the robot can make a turning motion. In order to provide a deflection angle of Cell 1, Cell 2 and Cell 3 are pasted between Cell 1 and Cell 4. When Cell 2 and Cell 3 inflate synchronously, Cell 1 is put up. Then, let Cell 2 and Cell 3 be with different radii, so Cell 1 get the deflection angle.

Figure 2 shows the experiment system, consisting of five spherical cells, the gas circuit system, microcon-

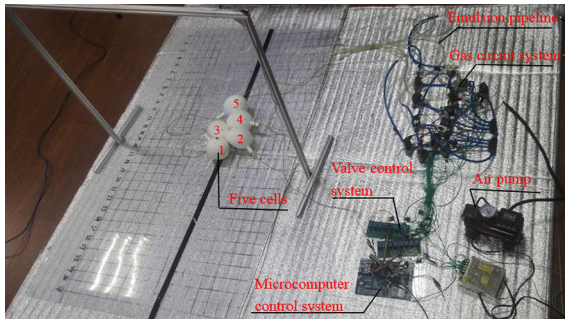

Fig. 2 A soft robot system consisting of five spherical cells

troller (AT89S52, ATMEL), the air pump (30 L/min), the solenoid valve (QVT307), the emulsion pipelines and power source (DC24V).

2.2 Inflation radius r

The five spherical cells are made of latex. In order to find the pressure property, we use Mooney–Rivlin model [18] to create the relation between the pressure P and the inflation radius r at different original radii r_0. The original thick of the spherical cell is h_0, which is much less than r_0. According to the Mooney–Rivlin model and the finite elasticity theory, we can obtain

$$\begin{cases} I_1 = \lambda_1^2 + \lambda_2^2 + \lambda_3^2 \\ I_2 = \lambda_1^{-2} + \lambda_2^{-2} + \lambda_3^{-2} \\ I_3 = \lambda_1\lambda_2\lambda_3 = 1 \end{cases} \tag{1}$$

where the stretches at three different directions are $\lambda_1 = \frac{h}{h_0}, \lambda_2 = \lambda_3 = \frac{r}{r_0}, \lambda_1 = \frac{1}{\lambda_2^2}$. I_i represents the principal invariant ($i = 1, 2, 3$). h represents the thick of each cell during the inflating and deflating process.

We can get the strain–energy density equation W.

$$\begin{aligned} W &= W(\lambda_1, \lambda_2, \lambda_3) = W(I_1, I_2, I_3) \\ &= W(I_1, I_2) - P(\lambda_1\lambda_2\lambda_3 - 1) \end{aligned} \tag{2}$$

We assume that all the cells remain spherical during the inflating and deflating process. We can obtain the relation between the inflation pressure P and the stretch $\lambda = \lambda_2 = \lambda_3$ due to the isotropic incompressible elastic property of latex cells [7].

$$P = \frac{4h_0}{r_0}\left(\lambda^{-1} - \lambda^{-7}\right)\left(\frac{\partial W}{\partial I_1} + \lambda^2\frac{\partial W}{\partial I_2}\right) = \frac{h_0}{r_0\lambda^2}\frac{\partial W}{\partial \lambda} \tag{3}$$

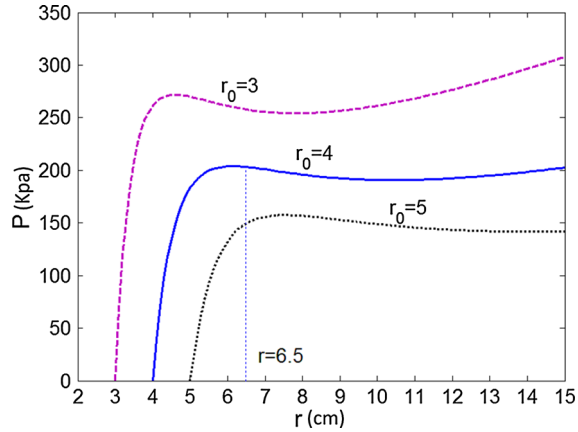

Fig. 3 Relation between pressure P and radius r

For Mooney–Rivlin material [18],

$$W = C_1(I_1 - 3) + C_2(I_2 - 3) \tag{4}$$

where C_1 and C_2 represent material constant. $C_1 = 1272$ kPa, $C_2 = 30$kPa.

According to (2), (3), (4), we can obtain

$$P = 4h_0[(r^6 - r_0^6)(C_1 r^{-7} - C_2 r_0^{-2} r^{-5})] \tag{5}$$

With (5), we can get Fig. 3 which shows the relation between pressure P and radius r. Three curves represent three different original radii r_0. In the paper, we choose the section of the curve where the pressure is increasing with radius, and also, we need to make sure the robot is small but with enough expansion rate. Thus, we design each cell with the original radius $r_0 = 4.0$ cm. In that case, the inflating radius of each spherical cell is from $r_0 = 4.0$ cm to $r = 6.5$ cm.

2.3 The velocity of inflation and deflation

At the inflating process, we use a constant-flow air pump to inflate the cell, and the rate of the flow is 30 L/min.

At the deflating process, we can obtain the velocity of deflation according to the Bernoulli's principle.

$$P_0 + \frac{1}{2}\rho v^2 = P \tag{6}$$

where P_0 is the atmospheric pressure, ρ is the air density, v is the velocity of exiting gas.

During the inflating or deflating process, each of the spherical cells is an independent compressed gas space.

We can use the ideal gas law of each cell.

$$P\mathrm{V} = nR\mathrm{T} \tag{7}$$

where $\mathrm{V} = \frac{4}{3}\pi r^3$, V is the volume of the individual spherical cell. R is the ideal gas constant which is 8.314 J/(k × mol) and T is Kelvin thermodynamic temperature, which is 273.15 K at zero temperature. n represents the number of moles.

At the inflating process $n = n_0 + \frac{qt}{V_m}$, n_0 is the number of moles at the original radius r_0, t is the inflation time, V_m represents the molar volume of gas, which is about 24 L/mole at 20 °C, q is the rate of the flow which is 30 L/min.

At the deflating process $n = n_1 - \frac{Svt}{V_m}$, n_1 is the number of moles at the radius r. S is the cross section of gas exit pipe.

According to (5) and (7), we can get the equation between the inflation radius r_I and the inflation time t, $r_I = r(t)$.

$$\frac{16}{3}\pi h_0\left[C_1\left({r_I}^2 - r_0^6 {r_I}^{-4}\right) + C_2\left(r_0^{-2}{r_I}^4 - r_0^4 {r_I}^{-2}\right)\right] = \frac{qtRT}{V_m} + n_0 RT \tag{8}$$

And according to (5), (6) and (7), we can obtain the equation between the deflation radius r_D and the deflation time t, $r_D = r(t)$.

$$\frac{16}{3}\pi h_0\left[C_1\left({r_D}^2 - r_0^6 {r_D}^{-4}\right) + C_2\left(r_0^{-2}{r_D}^4 - r_0^4 {r_D}^{-2}\right)\right] = n_1 RT - \frac{StRT}{V_m}\sqrt{2\frac{4h_0\left[C_1\left({r_D}^2 - r_0^6 {r_D}^{-4}\right) + C_2\left(r_0^{-2}{r_D}^4 - r_0^4 {r_D}^{-2}\right)\right] - P_0}{\rho}} \tag{9}$$

We can obtain the velocity of inflation and deflation.

$$v_r = \frac{dr\,(t)}{dt} \tag{10}$$

With (8) and (9), we can get the relation between the radius r and the inflation or deflation time t (the original radius $r_0 = 4.0$ cm), in Fig. 4a. And with (10), we can obtain the velocity of inflation and deflation in Fig. 4b.

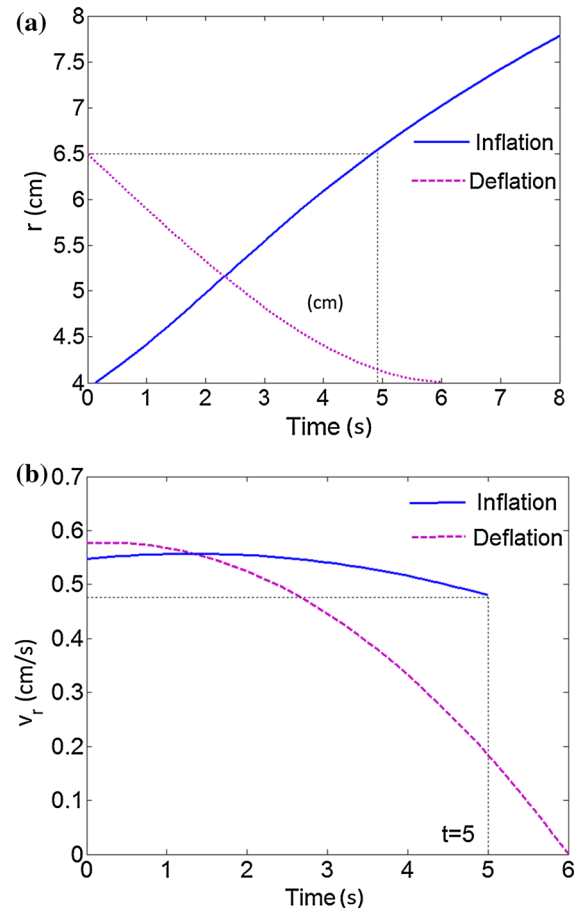

Fig. 4 **a** Relation between radius r and inflation or deflation time t. **b** Relation between velocity of inflation or deflation v_r and time t

3 Nonlinear turning motion analysis

3.1 Turning motion steps

The moving process of the multi-spherical modular soft robot depends on the deflating and inflating actions of each spherical cell. The whole deflating and inflating process is also largely related to the maximum radius and the minimum radius of each cell. The maximum radius of each spherical cell is $R_i = r = 6.5$ cm, and the minimum radius is $r_0 = 4$ cm. After the inflating and deflating process and two friction feet sticking with the ground in turn, the whole soft robot could turn and move forwards.

Five spherical cells are bonded as a whole soft robot. The center of Cell i is $O_i (i = 1, 2, 3, 4, 5)$. The fixed coordinates system OXYZ is set up. At the original state, O_5 is on the origin point O of the coordinates system OXYZ (Fig. 5). α represents the angle between the center line O_2O_4 (AB) and the center line O_3O_4, β represents the angle between the center line O_1O_2 and the center line O_1O_3, $\alpha = \beta = 90°$. The radii of the cells are the same, and the centers $O_1(E)$, $O_4(B)$,

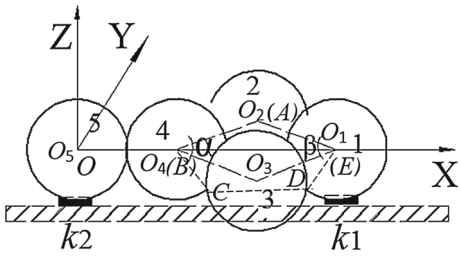

Fig. 5 Original state of the modular soft robot

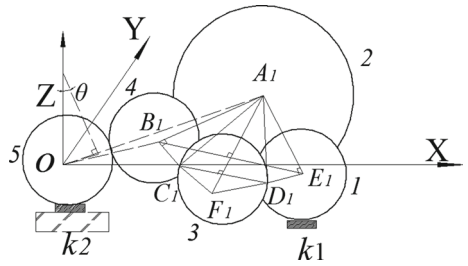

Fig. 6 Cell 2 inflating process

$O_5(O)$ are on the X-axis. Cell 3 is bonded with Cell 1 and Cell 4 at point C and point D.

We analyze the nonlinear turning motion of the modular soft robot. The turning process is divided into six steps in a period.

STEP A—The friction feet stick with the ground. Cell 2 and Cell 3 inflate (their radii change from 4 to 6.5 cm), and then, Cell 3 deflates (its radius changes from 6.5 to 4 cm). Thus, the friction foot k_1 is raised and Cell 1 gets a deflection angle.

STEP B—Cell 1 inflates (radius changes from 4 to 6.5 cm). Let the friction foot k_1 stick with the ground.

STEP C—Cell 4 inflates and its radius changes from 4 to 6.5 cm. Then, Cell 5 and the friction foot k_2 are raised.

STEP D—Cell 2 deflates and its radius changes from 6.5 to 4 cm. Because the friction foot k_1 sticks with the ground. Cell 5 and Cell 4 have a deflection. Thus, the whole robot has a deflection.

STEP E—Cell 1 deflates and its radius changes from 6.5 to 4 cm.

STEP F—Cell 4 deflates and its radius changes from 6.5 to 4 cm. The friction foot k_2 sticks with the ground. The five cells are back to the original state.

A period of the turning process is finished.

3.2 Nonlinear turning motion process

In Fig. 5, 1, 2, 3, 4, 5 stand for Cell 1, Cell 2, Cell 3, Cell 4, Cell 5, respectively, from the right to the left in the forward direction. Because the soft robot can finish the turning motion, the obstacles are placed in front of the robots and on the left of the robot on a flat surface. In a period, the turning motion process mainly consists of the following six steps.

STEP A—Cell 2 and Cell 3 inflate and then Cell 3 deflates.

In Fig. 6, in order to raise Cell 1 and the friction foot k_1, Cell 2 and Cell 3 inflate and then Cell 3 deflates. Thus, Cell 1 gets a deflection angle. At this step, Cell 2 and Cell 5 contact the ground. The centers of five cells are at the same plane Γ. The angle between Γ and the XOY plane is θ. At **STEP A**, because of the friction foot k_2 , only Cell 5 does not change its position. The centers of Cell 1, Cell 2, Cell 3 and Cell 4 are E_1, A_1, F_1 and B_1. The coordinates of each cell's center are as follows.

$$\theta_1(t) = \operatorname{asin}\left(\frac{r_2(t) - r_{05}}{r_{05} + r_{04} + \frac{\sqrt{2}}{2}r_{04} + \frac{\sqrt{2}}{2}r_2(t)}\right) \tag{11}$$

$$\tan\angle A_1B_1E_1 = \cot\angle B_1A_1F_1 = \frac{r_{04} + r_2(t)}{r_{04} + r_{03}} \tag{12}$$

$$\begin{cases} x_1^1(t) = \left[r_{05} + r_{04} + 2(r_{04} + r_2(t))\cos\angle A_1B_1E_1 \right. \\ \qquad \left. \cos\left(\angle A_1B_1E_1 - \frac{\pi}{4}\right)\right]\cos\theta_1(t) \\ y_1^1(t) = 2(r_{04} + r_2(t))\sin\angle A_1B_1E_1 \\ z_1^1(t) = \left[r_{05} + r_{04} + 2(r_{04} + r_2(t))\cos\angle A_1B_1E_1 \right. \\ \qquad \left. \cos\left(\angle A_1B_1E_1 - \frac{\pi}{4}\right)\right]\sin\theta_1(t) \end{cases} \tag{13}$$

$$\begin{cases} x_2^1(t) = \left[r_{05} + r_{04} + \frac{\sqrt{2}}{2}(r_{04} + r_2(t))\right]\cos\theta_1(t) \\ y_2^1(\mathrm{t}) = \frac{\sqrt{2}}{2}(r_{04} + r_2(t)) \\ z_2^1(t) = \left[r_{05} + r_{04} + \frac{\sqrt{2}}{2}(r_{04} + r_2(t))\right]\sin\theta_1(t) \end{cases} \tag{14}$$

$$\begin{cases} x_3^1 = \left[r_{05} + r_{04} + \frac{\sqrt{2}}{2}(r_{04} + r_{03})\right]\cos\theta_1(t) \\ y_3^1 = \frac{\sqrt{2}}{2}(r_{04} + r_{03}) \\ z_3^1 = \left[r_{05} + r_{04} + \frac{\sqrt{2}}{2}(r_{04} + r_{03})\right]\sin\theta_1(t) \end{cases} \tag{15}$$

$$\begin{cases} x_4^1 = (r_{05} + r_{04})\cos\theta_1(t) \\ y_4^1 = 0 \\ z_4^1 = (r_{05} + r_{04})\sin\theta_1(t) \end{cases} \tag{16}$$

$$\begin{cases} x_5^1 = 0 \\ y_5^1 = 0 \\ z_5^1 = 0 \end{cases} \tag{17}$$

x_i^j represents the x coordinates of Cell i at the j-th step. y_i^j represents the y coordinates of Cell i at the j-th step. z_i^j represents the z coordinates of Cell i at the j-th step. $r_i(t)$ represents Cell i's radius ($r_i = r = 6.5$ cm), r_{0i} represents Cell i's original radius ($r_{0i} = r_0 = 4.0$ cm).

STEP B—Cell 1 inflates (Fig. 7). Because of the friction foot k_2, the positions of the centers of Cell 2, Cell 3, Cell 4 and Cell 5 do not change. The center of Cell 1 is E_2. The coordinate of Cell 1's center is as follows.

$$\begin{cases} (x_1^2(t)-x_D)^2+(y_1^2(t)-y_D)^2+(z_1^2(t)-z_D)^2=r_1^2(t) \\ (x_1^2(t)-x_2^2)^2+(y_1^2(t)-y_2^2)^2+(z_1^2(t)-z_2^2)^2 \\ \quad =(r_1(t)+r_2)^2 \\ z_1^2(t)=r_1(t)-r_0 \end{cases} \tag{18}$$

$$\begin{cases} x_1^2(t)=\frac{P(t)-2y_1^2(t)(y_2^2-y_D)}{2(x_2^2-x_D)} \\ y_1^2(t)=\frac{-\eta(t)-\sqrt{\eta(t)^2-4\lambda\omega}}{2\lambda} \\ z_1^2(t)=r_1(t)-r_0 \end{cases} \tag{19}$$

Here

$$\begin{cases} P(t)=r_1(t)^2-(z_1^2-z_D)^2-(r_1(t)+r_2)^2 \\ \quad +(y_2^{2^2}+x_2^{2^2})-(x_D^2+y_D^2) \\ \lambda=1+\left(\frac{y_2^2-y_D}{x_2^2-x_D}\right)^2 \\ \eta(t)=-\left(2y_2^1-\frac{2(y_2^2-y_D)}{x_2^2-x_D}\left(x_2^1-\frac{P(t)}{2(x_2^2-x_D)}\right)\right) \\ \omega(t)=\left(x_2^1-\frac{P(t)}{2(x_2^2-x_D)}\right)^2+y_2^{2^2}-(r_1(t)+r_2)^2 \end{cases} \tag{20}$$

$$\begin{cases} \angle B_1A_1F_1=arc\tan\frac{r_{04}+r_{03}}{r_{04}+r_2} \\ \angle B_1A_1D_1=2\angle B_1A_1F_1-arc\tan\frac{r_{04}}{r_{04}+r_2} \\ A_1D_1=A_1C_1=\sqrt{(r_2+r_{04})^2+r_{04}^2} \\ B_1D_1= \\ \sqrt{(r_2+r_{04})^2+A_1D_1^2-2A_1D_1(r_2+r_{04})\cos\angle B_1A_1D_1} \\ \angle A_1B_1D_1=arc\sin\left(\frac{A_1D_1}{B_1D_1}\sin\angle B_1A_1D_1\right) \end{cases} \tag{21}$$

$$\begin{cases} x_D=\left[r_{05}+r_{04}+B_1D_1\cos\left(\angle A_1B_1D_1-\frac{\pi}{4}\right)\right]\cos\theta \\ y_D=B_1D_1\sin\left(\angle A_1B_1D_1-\frac{\pi}{4}\right) \\ z_D=\left[r_{05}+r_{04}+B_1D_1\cos\left(\angle A_1B_1D_1-\frac{\pi}{4}\right)\right]\sin\theta \end{cases} \tag{22}$$

$$\begin{cases} x_2^2=x_2^1 \\ y_2^2=y_2^1 \\ z_2^2=z_2^1 \end{cases} \tag{23}$$

After Cell 1 finishes inflating, its friction foot k_1 sticks with the ground. At the next steps of the turning motion process, the coordinate of Cell 1's center will not change. The deflections of the robot head are as follows.

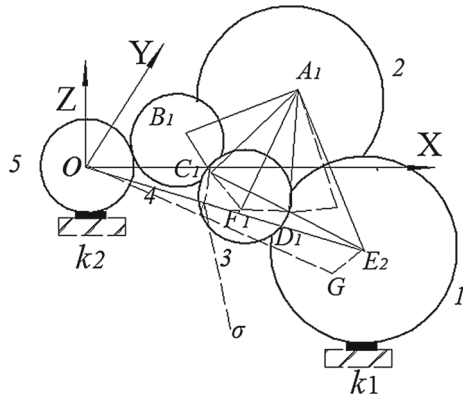

Fig. 7 Cell 1 inflating process

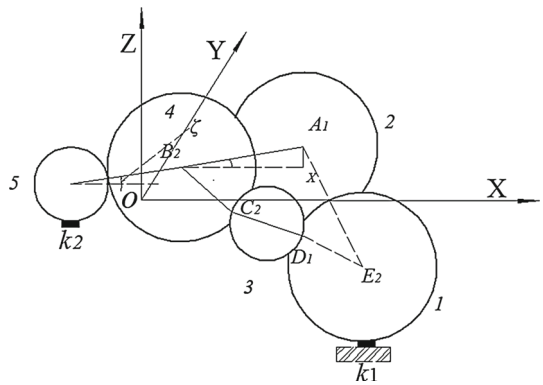

Fig. 8 Cell 4 inflating process

$$\begin{cases} \Delta x=x_1^2-\left(2+2\sqrt{2}\right)r_0 \\ \Delta y=y_1^2 \\ \Delta z=z_1^2=r_1-r_0 \end{cases} \tag{24}$$

STEP C—Cell 4 inflates. During the inflating process of Cell 4, in order to simplify the model, the tiny deflection of Cell 4 in the Y-axis direction is ignored. Because of the friction foot k_1, the coordinates of Cell 1's center and Cell 2's center do not change. ζ represents the angle between the center line O_5B_2 and the XOY plane, in Fig. 8. The coordinates of Cell 4's center and Cell 5's center are as follows.

$$\angle A_1B_2X=arcsin\frac{y_2^3}{r_4(t)+r_2} \tag{25}$$

$$\begin{cases} x_2^3=x_2^1 \\ y_2^3=y_2^1 \\ z_2^3=z_2^1 \end{cases} \tag{26}$$

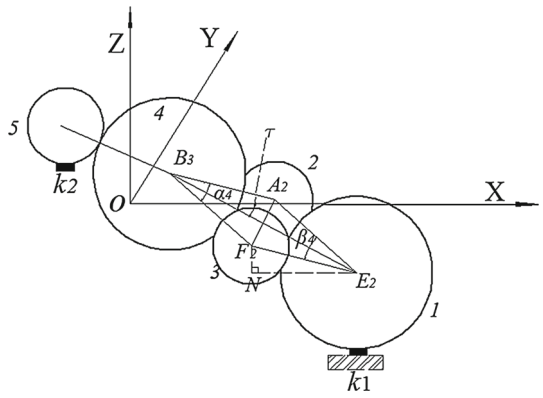

Fig. 9 Cell 2 deflating process

$$\begin{cases} x_4^3(t) = x_2^3 - (r_4(t) + r_2)\cos\angle A_1B_2X \\ y_4^3 = 0 \\ z_4^3(t) = r_4(t) - r_{05} \end{cases} \tag{27}$$

$$\begin{cases} x_5^3(t) = x_4^3(t) - (r_4(t) + r_{05})\cos\zeta \\ y_5^3 = 0 \\ z_5^3(t) = r_4(t) - r_{05} - (r_4(t) + r_{05})\sin\zeta \end{cases} \tag{28}$$

STEP D– Cell 2 deflates.

In Fig. 9, the friction foot k_1 sticks with the ground, so the positions of Cell 1 and Cell 3 do not change. The centers of the five cells are at the same plane. After Cell 2 finishes deflating, the distance between Cell 2's center and Cell 3's center is back to the original state, as $A_2F_2 = 2\sqrt{2}r_0$. τ represents the deflection angle of the soft robot, which is the angle between the center line O_5O_1 and the X-axis in XOY plane. And the coordinates of each cell are as follows.

$$\begin{cases} \alpha_4(t) = \beta_4(t) = 2arc\sin\left(\frac{\sqrt{2}r_2(t)}{r+r_2(t)}\right) \\ \angle F_2E_2N = arctan\frac{y_3^4 - y_1^4}{x_1^4 - x_3^4} \\ \tau(t) = \angle F_2E_2N + \frac{1}{2}\beta_4(t) \end{cases} \tag{29}$$

$$\begin{cases} x_1^4 = x_1^2 \\ y_1^4 = y_1^2 \\ z_1^4 = r - r_0 \end{cases} \tag{30}$$

$$\begin{cases} x_2^4(t) = x_1^4 - (r_1 + r_{03})\cos\left(\tau(t) + \frac{1}{2}\beta_4(t)\right) \\ y_2^4(t) = y_1^4 + (r_1 + r_{03})\sin\left(\tau(t) + \frac{1}{2}\beta_4(t)\right) \\ z_2^4 = r - r_0 \end{cases} \tag{31}$$

$$\begin{cases} x_3^4 = x_3^1 \\ y_3^4 = y_3^1 \\ z_3^4 = r - r_0 \end{cases} \tag{32}$$

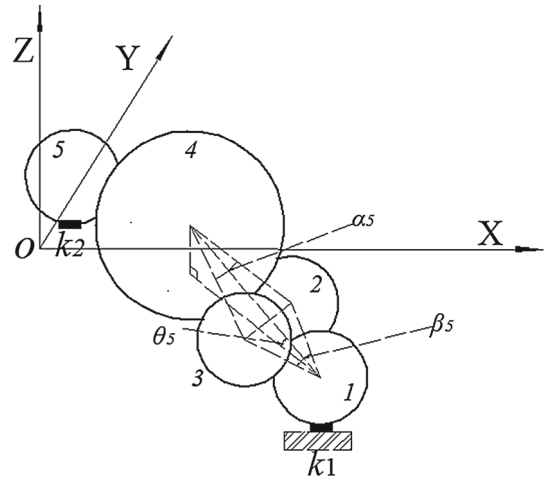

Fig. 10 Cell 1 deflating process

$$\begin{cases} x_4^4 = x_1^4 - (r_4 + r_{03})\cos\frac{\alpha_4(t)}{2}\cos\tau(t) \\ y_4^4 = y_1^4 + (r_4 + r_{03})\cos\frac{\alpha_4(t)}{2}\sin\tau(t) \\ z_4^4 = r - r_0 \end{cases} \tag{33}$$

$$\begin{cases} x_5^4 = x_4^4 - (r_4 + r_{05})\cos\tau(t) \\ y_5^4 = y_4^4 + (r_4 + r_{05})\sin\tau(t) \\ z_5^4 = r - r_0 \end{cases} \tag{34}$$

STEP E– Cell 1 deflates.

In Fig. 10, after Cell 1 finishes deflating, Cell 1 and its friction foot k_1 stick with the ground, the centers of the five cells are at the same plane Γ', and the intersection angle between the plane Γ ' and the XOY plane is θ_5. β_5 is back to the original state, $\beta_5 = 90°$. The coordinates of Cell 4's center and Cell 5's center are as follows.

$$\theta_5(t) = arcsin\frac{r_4 - r_1(t)}{(r_4 + r_{03})cos\frac{\alpha_5}{2} + (r_{03} + r_1(t))cos\frac{\beta_5(t)}{2}} \tag{35}$$

$$\begin{cases} \beta_5(t) = 2arc\sin\left(\frac{\sqrt{2}r_1(t)}{r+r_1(t)}\right) \\ \alpha_5 = 2arcsin\frac{\sqrt{2}r_{03}}{(r_4+r_{03})} \end{cases} \tag{36}$$

$$\begin{cases} x_1^5 = x_1^2 \\ y_1^5 = y_1^2 \\ z_1^5(t) = r_1(t) - r_0 \end{cases} \tag{37}$$

$$\begin{cases} x_4^5(t) = x_1^5 - \sqrt{2}r_{03}\left(cot\frac{\alpha_5}{2} + cot\frac{\beta_5(t)}{2}\right)cos\theta_5(t)cos\tau \\ y_4^5(t) = y_1^5 + \sqrt{2}r_{03}\left(cot\frac{\alpha_5}{2} + cot\frac{\beta_5(t)}{2}\right)cos\theta_5(t)\sin\tau \\ z_4^5 = r - r_0 \end{cases} \tag{38}$$

$$\begin{cases} x_5^5(t) = x_4^5 - (r_4 + r_{05})cos\theta_5(t)cos\tau \\ y_5^5(t) = y_4^5 + (r_4 + r_{05})cos\theta_5(t)\sin\tau \\ z_5^5(t) = \left[r_4 + r_{05} + \sqrt{2}r_{03}\left(cot\frac{\alpha_5(t)}{2} + cot\frac{\beta_5(t)}{2}\right)\right]sin\theta_5(t) \end{cases} \tag{39}$$

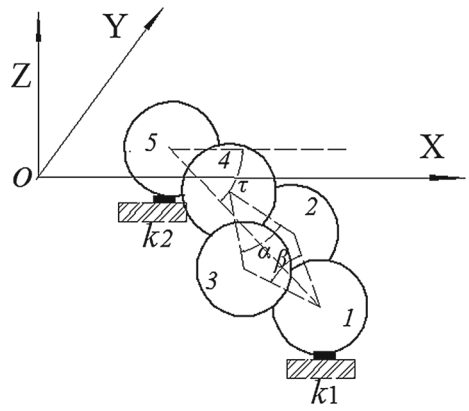

Fig. 11 Cell 4 deflating process

STEP F—Cell 4 deflates.

In Fig. 11, after Cell 4 finishes deflating, a period of the turning process is finished and five cells are back to the original state. The coordinates are as follows.

$$\theta_6(t) = arcsin \frac{r_4(t) - r_{01}}{(r_4(t) + r_{03}) cos\frac{\alpha_6(t)}{2} + (r_{03} + r_{01}) cos\frac{\beta_6}{2}} \tag{40}$$

$$\begin{cases} \alpha_6(t) = 2arc\sin\left(\frac{\sqrt{2}r_4(t)}{r+r_4(t)}\right) \\ \beta_6 = 2arcsin\frac{\sqrt{2}r_{03}}{(r_{01}+r_{03})} \end{cases} \tag{41}$$

$$\begin{cases} x_1^6 = x_1^2 \\ y_1^6 = y_1^2 \\ z_1^6 = 0 \end{cases} \tag{42}$$

$$\begin{cases} x_4^6 = x_1^6 - \left[\frac{\sqrt{2}}{2}(r_{01} + r_{02}) + (r_4(t) + r_{02})\cos\alpha_6(t)\right]\cos\tau \\ y_4^6 = y_1^6 + \left[\frac{\sqrt{2}}{2}(r_{01} + r_{02}) + (r_4(t) + r_{02})\cos\alpha_6(t)\right]\sin\tau \\ z_4^6 = r_4(t) - r_0 \end{cases} \tag{43}$$

$$\begin{cases} x_5^6 = x_1^6 - \left[\frac{\sqrt{2}}{2}(r_{01} + r_{02}) + (r_4(t) + r_{02})\right. \\ \qquad \left.\cos\alpha_6(t) + r_{05} + r_4(t)\right]\cos\tau \\ y_5^6 = y_1^6 + \left[\frac{\sqrt{2}}{2}(r_{01} + r_{02}) + (r_4(t) + r_{02})\right. \\ \qquad \left.\cos\alpha_6(t) + r_{05} + r_4(t)\right]\sin\tau \\ z_5^6 = r_4(t) - r_0 \end{cases} \tag{44}$$

In one period, we obtain the deflection angle of the soft robot $\tau \approx 26°$. Iterating the above six steps, the soft robot can finish the turning motion.

In Fig. 12, using Cell 1 as the research object, we can obtain the coordinates (x_1, y_1, z_1) and velocities of Cell 1's center. At each step, the inflating time is 5 s, the deflating time is 6 s.

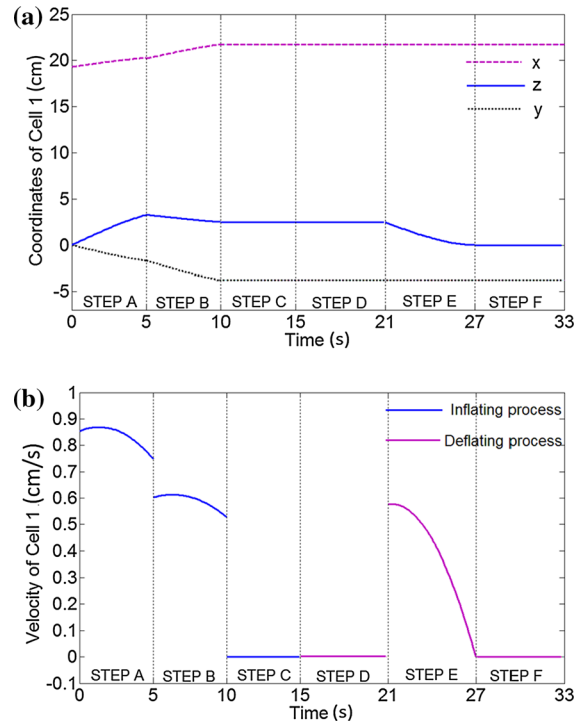

Fig. 12 **a** Coordinates of Cell 1 at one cycle (six steps). **b** The velocity of Cell 1 at one cycle

The velocity (v_r) of Cell 1's center at each step can be described as

$$v_r = \sqrt{v_x^2 + v_y^2 + v_z^2} \tag{45}$$

4 Simulation and experiment

The soft robot consists of five deformable spherical cells and two friction feet (Fig. 13). The different inflating and deflating sequences of five cells and two friction feet sticking with the ground make the soft robot perform a turning motion and avoid obstacles.

We use PYTHON language to finish the simulation. In the simulation and experiment, the soft body would inflate and deflate with the above six steps, and the turning direction is in clockwise direction. In Fig. 13a, the soft robot moves according to **STEP A**. Cell 2 and Cell 3 inflate and then Cell 3 deflates. Thus, Cell 1 gets a deflection angle. After that, Cell 1 inflates. The friction foot k_1 sticks with the ground. The soft robot works according to **STEP B** (Fig. 13b). Then, Cell 4 inflates. Because of the increase in Cell 4' radius, Cell 5 and the friction foot k_2 are raised (Fig. 13 c). **STEP C** is

finished. In Fig. 13d, the soft robot turns according to **STEP D**. Cell 2 deflates. Cell 5 and Cell 4 have a deflection. Thus, the whole robot has a deflection. After that, in **STEP E,** Cell 1 deflates (Fig. 13e). In the last **STEP F**, Cell 4 deflates (Fig. 13f). The five cells are back to the original state. A period of the turning process is finished. By these special processes, the soft robot makes a turning motion about 20°. Then, the robot continues working according to **STEP A**. Table 1 shows the deflection angle τ of the soft robot at each step in the simulation and the experiment. The total time in one period is 33 s. The efficiency of the soft robot turning motion is 76.9%. The error comes from the friction of Cell 2, Cell 3 and Cell 4, which is ignored in the theoretical model.

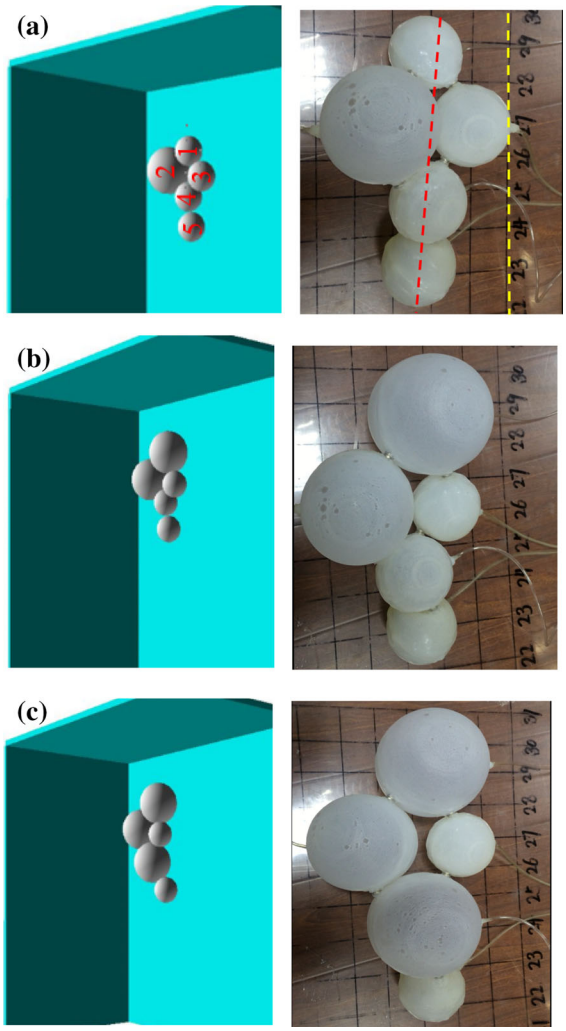

Fig. 13 Simulation and experiment of making a turning motion (**a**) The soft robot works according to **STEP A**. **b** The soft robot works according to **STEP B**. **c** The soft robot works according to **STEP C**. **d** The soft robot works according to **STEP D**. **e** The soft robot works according to **STEP E**. **f** The soft robot works according to **STEP F**

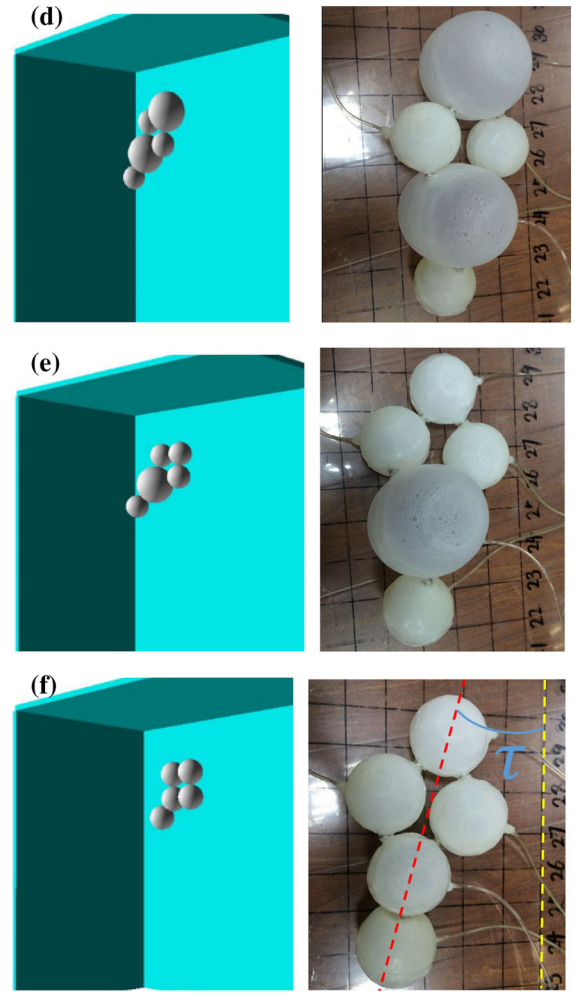

Fig. 13 continued

Table 1 Deflection angle τ of soft robot

	Simulation (°)	Experiment (°)	Time (s)
STEP A	10	6	5
STEP B	16	13	10
STEP C	13	11	15
STEP D	26	18	21
STEP E	26	18	27
STEP F	26	20	33

5 Conclusions

The soft robot consists of several deformable spherical cells and friction feet. According to the deflating action and the inflating action of the cells, and each friction foot sticking with the ground, the soft robot can change the size and the shape to move forwards, make a turning motion and avoid obstacles. The nonlinear relation between the pressure P and the inflation radius (r) at different original radii (r_0) is analyzed, and the inflation and deflation velocity v_r is obtained. In a period, six inflating and deflating steps to finish the turning motion are presented. Based on the geometric relationship between the inflation radius (r) and the original diameters (r_0) of each cell, the nonlinear turning process is described to control the positions' change of the spherical cells. Last, a simulation and an experiment are shown to emulate the turning process of the soft robot and perform the soft robot to turn and avoid the obstacle. Experiment results show that the robot has a maximum turning capability of 20 degrees in one period with the efficiency of 76.9%. The error comes from the friction of Cell 2, Cell 3 and Cell 4, which is ignored in the theoretical model. In order to reduce the frictional effect of Cell 2, Cell 3 and Cell 4 and increase the efficiency, the future work will focus on the smoothness and lightness of the spherical cells' material and the improvement of the friction force on friction feet.

Acknowledgements This research was supported by National Natural Science Foundation of China (Grant No. 51475300) and Open Foundation of First Level Zhejiang Key in Key Discipline of Control Science and Engineering.

References

1. Kim, S., Laschi, C., Trimmer, B.: Soft robotics: a bioinspired evolution in robotics. Trends Biotechnol. **31**(5), 287–294 (2013)
2. Fei, Y.Q., Shen, X.Y.: Nonlinear analysis on moving process of soft robots. Nonlinear Dyn. **73**(1–2), 672–677 (2013)
3. Trimmer, B., Lin, H., Amanda, B., Leisk, G. G., Kaplan, D. L.: Towards a biomorphic soft robot: design constraints and solutions. In: Proceedings 4th International Conference on Biomedical Robotics and Biomechatronics (BioRob). Rome, Italy, pp. 599–605. (2012)
4. Onal, C.D., Rus, D.: Autonomous undulatory serpentine locomotion utilizing body dynamics of a fluidic soft robot. Bioinspiration Biomim. **8**(2), 026003 (2013)
5. Cecilia, L., Matteo, C., Barbara, M., Laura, M., Maurizio, F., Paolo, D.: Soft robot arm inspired by the octopus. Adv. Robot. **26**, 709–727 (2012)
6. Manti, M., Hassan, T., Passetti, G., D'Elia, N., Cianchetti, M., Laschi, C.: An under-actuated and adaptable soft robotic gripper. Biomim. Biohybrid Syst. **9222**, 64–74 (2015)
7. Fei, Y.Q., Gao, H.W.: Nonlinear dynamic modeling on multi-spherical modular soft robots. Nonlinear Dyn. **78**, 831–838 (2014)
8. Calisti, M., Arienti, A., Renda, F., Levy, G., Hochner, B., Mazzolai, B., Dario, P., Laschi, C.: Design and development of a soft robot with crawling and grasping capabilities. In: Proceedings of 2012 IEEE International Conference Robotics Automation, pp. 4950–4955. Saint Paul, MN. (2012)
9. Koizumi, Y., Shibata, M., Hirai, S.: Rolling tensegrity driven by pneumatic soft actuators. Proceedings of 2012 IEEE International Conference Robotics Automation, pp. 1988–1993 . Saint Paul, MN (2012)
10. Sugiyama, Y., Hirai, S.: Crawling and jumping by a deformable robot. Int. J. Robot. Res. **25**(5–6), 603–620 (2006)
11. Yao, J., Di, D., Gao, S., He, L., Hu, S.: Sliding mode control scheme for a jumping robot with multi-joint based on floating basis. Int. J. Control **85**(1), 41–49 (2012)
12. Marchese, A., D., Onal, C. D., Rus, D.: Soft robot actuators using energy-efficient valves controlled by electropermanent magnets. In: Proceedings of IEEE/RSJ International Conference Intelligent Robots Systems, pp. 756–761. San Francisco, CA (2011)
13. Teruyoshi, O., Taro, N.: Path tracking method for traveling-wave-type omnidirectional mobile robot (TORoIII). J. Robot. Mech. **24**(2), 340–346 (2012)
14. Koh, J., Lee, D., Kim, S., Cho, K.: Deformable soft wheel robot using hybrid actuation. In: Proceedings of IEEE/RSJ International Conference Intelligent Robots System, pp. 3869–3870. (2012)
15. Hou, J.P., Lou, M.Z., Luo, T., M.: The design and control of amoeba-like robot. In: Proceedings of International Conference on Computer Application and System Modeling, pp. 8–91. ICCASM, Shan Xi. China (2010)
16. Shepherd, R.F., Stokes, A.A., Freake, J., et al.: Using explosions to power a soft robot. Angewandte Chem. **125**(10), 2892–2896 (2013)
17. Huang, C., Lv, J. A., Tian, X., Wang, Y., Yu, Y., Liu, J.: Miniaturized swimming soft robot with complex movement actuated and controlled by remote light signals. Scientific reports 5 (2015)
18. Beatty, M.F.: Topics in finite elasticity: hyperelasticity of rubber, elastomers, and biological tissues—with examples. Appl. Mech. Rev. **40**, 1699–1734 (1987)